



HAL
open science

Sensitivity of global terrestrial carbon cycle dynamics to variability in satellite-observed burned area

Benjamin Poulter, Patricia Cadule, Audrey Cheiney, Philippe Ciais, Elke Hodson, Philippe Peylin, Stephen Plummer, Allan Spessa, Sassan Saatchi, Chao Yue, et al.

► To cite this version:

Benjamin Poulter, Patricia Cadule, Audrey Cheiney, Philippe Ciais, Elke Hodson, et al.. Sensitivity of global terrestrial carbon cycle dynamics to variability in satellite-observed burned area. *Global Biogeochemical Cycles*, 2015, 29 (2), pp.207 - 222. 10.1002/2013GB004655 . hal-01806221

HAL Id: hal-01806221

<https://hal.science/hal-01806221>

Submitted on 28 Oct 2020

HAL is a multi-disciplinary open access archive for the deposit and dissemination of scientific research documents, whether they are published or not. The documents may come from teaching and research institutions in France or abroad, or from public or private research centers.

L'archive ouverte pluridisciplinaire **HAL**, est destinée au dépôt et à la diffusion de documents scientifiques de niveau recherche, publiés ou non, émanant des établissements d'enseignement et de recherche français ou étrangers, des laboratoires publics ou privés.



Global Biogeochemical Cycles

RESEARCH ARTICLE

10.1002/2013GB004655

Key Points:

- Fire as a component of the earth system is overlooked in carbon cycle models
- Satellite-derived burned area can inform fire model development in DGVM models
- Fire controls carbon-vegetation feedbacks that affect initial model conditions

Supporting Information:

- Readme
- Figure S1
- Table S1
- Table S2
- Table S3
- Table S4

Correspondence to:

B. Poulter,
benjamin.poulter@montana.edu

Citation:

Poulter, B., et al. (2015), Sensitivity of global terrestrial carbon cycle dynamics to variability in satellite-observed burned area, *Global Biogeochem. Cycles*, 29, 207–222, doi:10.1002/2013GB004655.

Received 20 MAY 2013

Accepted 11 JAN 2015

Accepted article online 14 JAN 2015

Published online 25 FEB 2015

Sensitivity of global terrestrial carbon cycle dynamics to variability in satellite-observed burned area

Benjamin Poulter^{1,2}, Patricia Cadule², Audrey Cheiney², Philippe Ciais², Elke Hodson³, Philippe Peylin², Stephen Plummer⁴, Allan Spessa⁵, Sassan Saatchi⁶, Chao Yue², and Niklaus E. Zimmermann³

¹Institute on Ecosystems and Department of Ecology, Montana State University, Bozeman, Montana, USA, ²Laboratoire des Sciences du Climat et de l'Environnement, LSCE CEA CNRS UVSQ, Gif Sur Yvette, France, ³Dynamic Macroecology, Swiss Federal Research Institute WSL, Birmensdorf, Switzerland, ⁴ESA Climate Office, European Space Agency – Harwell, Oxfordshire, UK, ⁵Department of Environment, Earth and Ecosystems, Open University, Milton Keynes, UK, ⁶Jet Propulsion Laboratory, California Institute of Technology, Pasadena, California, USA

Abstract Fire plays an important role in terrestrial ecosystems by regulating biogeochemistry, biogeography, and energy budgets, yet despite the importance of fire as an integral ecosystem process, significant advances remain to improve its prognostic representation in carbon cycle models. To recommend and to help prioritize model improvements, this study investigates the sensitivity of a coupled global biogeography and biogeochemistry model, LPJ, to observed burned area measured by three independent satellite-derived products, GFED v3.1, L3JRC, and GlobCarbon. Model variables are compared with benchmarks that include pantropical aboveground biomass, global tree cover, and CO₂ and CO trace gas concentrations. Depending on prescribed burned area product, global aboveground carbon stocks varied by 300 Pg C, and woody cover ranged from 50 to 73 Mkm². Tree cover and biomass were both reduced linearly with increasing burned area, i.e., at regional scales, a 10% reduction in tree cover per 1000 km², and 0.04-to-0.40 Mg C reduction per 1000 km². In boreal regions, satellite burned area improved simulated tree cover and biomass distributions, but in savanna regions, model-data correlations decreased. Global net biome production was relatively insensitive to burned area, and the long-term land carbon sink was robust, ~2.5 Pg C yr⁻¹, suggesting that feedbacks from ecosystem respiration compensated for reductions in fuel consumption via fire. CO₂ transport provided further evidence that heterotrophic respiration compensated any emission reductions in the absence of fire, with minor differences in modeled CO₂ fluxes among burned area products. CO was a more sensitive indicator for evaluating fire emissions, with MODIS-GFED burned area producing CO concentrations largely in agreement with independent observations in high latitudes. This study illustrates how ensembles of burned area data sets can be used to diagnose model structures and parameters for further improvement and also highlights the importance in considering uncertainties and variability in observed burned area data products for model applications.

1. Introduction

Following climatic controls in determining global patterns of biogeography, the distribution of terrestrial ecosystems worldwide is largely influenced by interactions with fire [Archibald et al., 2013; Bond et al., 2005]. Fire acts as a process that delineates boundaries between biomes, influences the structure and composition of ecosystems [Poulter et al., 2008; Randerson et al., 2006; Schulze et al., 2012; Staver et al., 2011], and affects the evolution of biota [Bond and Keely, 2005; Verdu et al., 2007]. Fire rapidly alters the carbon and energy balance of ecosystems, especially during drought years, turning regional carbon sinks to carbon sources [Aragão et al., 2008; Bowman et al., 2009; Nowacki and Abrams, 2008; Page et al., 2002; Randerson et al., 2006]. At the global scale, interannual anomalies of carbon emissions from fire, as high as 1–2 Pg C yr⁻¹ [van der Werf et al., 2010], can impose their signature on the background rate of atmospheric CO₂ growth from anthropogenic fossil fuel emissions, for example, during El Niño years [Langenfelds et al., 2002; Page et al., 2002; Peters et al., 2011]. Thus, monitoring long-term trends and the interannual variability of burned area is an important component in observing systems that document changes in the global carbon cycle [Ciais et al., 2013].

Current observation systems for fire monitoring must overcome several issues related to where satellite observations cover time periods that are often too short [Arino et al., 2011; Kasischke et al., 2011] or in cases where historical documents used to reconstruct burned area over longer-time periods are associated with

high uncertainty [Mouillot and Field, 2005]. To address these limitations, numerical fire models have a promising role to assist in hindcasting or forecasting changes in fire regimes and subsequent interactions with vegetation and trace gas emissions over large spatial and temporal domains [Prentice et al., 2011; Schultz et al., 2008]. Numerical, or process-based, modeling of fire requires a detailed description of physical principles related to ignitions, fire spread, and fire effects on vegetation mortality and trace gas emissions [Liu et al., 2011; Pechony and Shindell, 2009]. At each stage of modeling the fire process, model structure and parameters are associated with different sources of uncertainty due to either stochastic factors, such as ignitions, or fine-scale variability and heterogeneity in plant traits or landscape features, which become aggregated during simulations.

One of the largest sources of uncertainty is the modeling of successful fire ignitions that occur when fuel loading, fuel moisture, and ignition sources converge, i.e., the fire “triangle.” Ignitions from lightning and human activities, whether accidental or intentional, have well-known large interannual and spatial variability [Krause et al., 2014; Pfeiffer et al., 2013] and include interactions with socioeconomic factors related to fire suppression or prescribed fire that can change over time as land management policies evolve [Costa et al., 2011; Marlon et al., 2008; Prentice et al., 2011; Ryan et al., 2013]. While the physical principles that determine the spread of fire are relatively well established, as encapsulated by *Rothermel* [1972], the rate of spread is influenced by fine-scale landscape features that act as natural fire breaks (i.e., rivers and lakes) that are generally ignored in ecosystem-based fire models. Postfire mortality and the combustion of biomass to trace gas ensembles [Andreae and Merlet, 2001] is also influenced by a range of factors, including interactions between fire intensity [Kaiser et al., 2012], in kW m^{-1} , with tree diameter and crown structure as well as plant traits adapted to fire. In most carbon cycle models, the scaling of plant properties leads inevitably to simplified assumptions related to modeling fire-vegetation effects, for example, where single “big-leaf,” rather than multilayer, forest canopy profiles exist, or where the aggregation of species with a range of diverse traits is represented by a subset of plant functional types (PFT).

Several “prognostic” fire modules are now used within carbon cycle models with the main aim to provide estimates of burned area and trace gas emissions, and with an increasing interest in understanding effects of fire on vegetation patterns and mineral or organic soil properties. These modules can be found within CLM [Kloster et al., 2010; Li et al., 2012], LPJ [Thonicke et al., 2001, 2010; Venevsky et al., 2002], LPX [Prentice et al., 2011], SDGVM [Quegan et al., 2011], CTEM [Arora and Boer, 2005], MC1 [Bachelet et al., 2000], ORCHIDEE [Yue et al., 2014], and GFED-CASA [van der Werf et al., 2003], for example. Fire modules are distinguished from one another by structure and the degree of complexity of physical processes related to fire behavior and fire effects on vegetation. Some modules require prescribed satellite observations of burned area, such as GFED-CASA, whereas other modules are prognostic and use either semiempirical or fully mechanistic processes to estimate burned area. Common to all modules are processes where fire consumes live vegetation and dead fuels to estimate emissions, and for those models with dynamic vegetation, fire can alter the potential distribution of plant functional types (PFT). This feedback between fire and vegetation patterns is particularly important because it influences the distribution of aboveground biomass, net primary production, and ultimately, the future characteristics of fuel loading. Because of these feedbacks, improving the numerical representation of fire-vegetation interactions has important implications that could result in improvement of a range of ecosystem processes.

Here, we focus on the role of burned area in improving fire models, building on recent work by *Lehsten et al.* [2008], who demonstrated the importance of using observed burned area for estimating trace gas emissions over Africa using the LPJ-GUESS model. The authors found that observed burned area, from the L3JRC satellite data [Tansey et al., 2008], follows a unique unimodal response to precipitation, a response function that can be used not only as a benchmark for prognostic models but also applied empirically to achieve realistic emission estimates. In a follow-up exercise, *Knorr et al.* [2012] showed, using LPJ-GUESS, that trace gas emissions depend strongly on the particular burned area data set by contrasting L3JRC with the MODIS burned area product used within GFED-CASA [Giglio et al., 2010], and that improvements in combustion efficiencies may be as important as improving burned area estimation. These studies demonstrated the various ways in how discrepancies between burned area data can propagate to trace gas emission estimates but did not address the sensitivity of feedbacks between burned area, vegetation, and carbon stocks. At present, satellite-derived burned area remains one of the most useful fire-related variables to integrate within fire models because it is available from several optical remote-sensing satellites where their bias and

Table 1. Description of the Main Spatial and Temporal Characteristics of the Burned Area Satellite Products Used as External Forcing for the LPJ-wsl Model

| Burned Area Product | Satellite Sensor | Time Period | Native Spatial Resolution | Reference |
|---------------------|------------------------------|-------------|---------------------------|------------------------------|
| GlobCarbon | SPOT VEGETATION | 1998–2007 | 0.5° | <i>Plummer et al.</i> [2007] |
| L3JRC | SPOT VEGETATION | 2000–2007 | 0.0083° | <i>Tansey et al.</i> [2008] |
| MODIS-GFED | MODIS Terra/Aqua (TRMM/VIRS) | 1997–2009 | 0.5° | <i>Giglio et al.</i> [2009] |

uncertainty has been relatively well established [Chang and Song, 2009; Giglio et al., 2010; Kasischke et al., 2011]. A multidata product approach can also be informative for both understanding the sensitivity of modeled ecosystem processes to differences in burned area as well as for evaluating the performance of burned area data sets during model benchmarking.

This study uses the LPJ dynamic global vegetation model [Sitch et al., 2003] as a modeling framework to integrate observed burned area data from three different satellite products, L3JRC [Tansey et al., 2008], MODIS-GFED [Giglio et al., 2010], and GlobCarbon [Plummer et al., 2007]. The objective was to determine the sensitivity of modeled tree cover, carbon stocks, and CO and CO₂ fluxes to differences in burned area and to target model processes and parameters for model development. The distributions for simulated tree cover are compared with a gridded PFT database [Poulter et al., 2011], pantropical carbon stocks are compared with satellite-derived biomass estimates [Saatchi et al., 2011], and CO (carbon monoxide) and CO₂ fluxes are transported to compare with a tower observation network [Pison et al., 2009].

2. Methods

2.1. Satellite Data

Observed burned area data were prepared as “diagnostic” inputs for LPJ DGVM simulations from three satellite products (Table 1). Because of challenges in mapping burned area from space, burned area remote sensing products vary considerably from one another as shown in several burned-area comparison studies, e.g., Giglio et al. [2010] and Kasischke et al. [2011]. Several processes involved in developing these data sets are responsible for the differences, mainly, the type of fire detection algorithm, the sensor and orbit specifications that determine the time of day of the overpass, and spectral, spatial, and temporal resolution. These processes can contribute to the omission of burned area via influences on minimum fire size detection, and missing fires with short duration, or fires obscured by cloud cover.

Of the products used in this study, MODIS-GFED (v3.1) is produced using daily 500 m Collection 5 MODIS surface reflectance and daily active fire count data [Giglio et al., 2010] with locally trained regression models to estimate burned area from “hot,” pixels. The MODIS-GFED data are provided monthly, at 0.5° spatial resolution, from 1997 to 2009 with pre-MODIS era data recorded by Tropical Rainfall Measuring Mission (TRMM) – Visible and Infrared Scanner (VIRS) and European Remote Sensing Satellites (ERS) Along Track Scanning Radiometer (ATSR) sensors. L3JRC uses daily 1 km SPOT VEGETATION surface reflectance data from the SPOT 4 satellite [Tansey et al., 2008]. A global burn detection algorithm is used to classify burned pixels using data from the near-infrared bands, producing a 1 km resolution product specifying the day of year a pixel was burned. For L3JRC, we calculated monthly 0.5° resolution burned area by converting day of year to month and then aggregating to the coarser resolution grid cell boundaries. The third burned area data set was produced during the GlobCarbon project coordinated by the European Space Agency [Plummer et al., 2007]. GlobCarbon is a multisensor product using surface reflectance data from ATSR2, AATSR, SPOT, and three separate burned area-mapping algorithms, to assess agreement, that are applied globally. It is provided to users at a monthly time step at either 1 km or 10 km, or as used in this study 0.5° spatial resolution.

2.2. LPJ Dynamic Global Vegetation Model

The LPJ-wsl dynamic global vegetation model (DGVM) originates from LPJv3.1 developed by Sitch et al. [2003] and includes modifications to hydrologic processes as described by Gerten et al. [2004]. For this study, LPJ-wsl, where “wsl” denotes minor modifications to the main “trunk” of LPJ made at the Swiss Federal Institute WSL, was adapted to ingest the diagnostic monthly burned area inputs and to also include an estimation of a range of trace gas emissions during fire. LPJ-wsl uses the GlobFirm fire module, developed and benchmarked by Thonicke et al. [2001], to estimate burned area and subsequent fire effects on vegetation. The implementation of trace gas emission calculations followed Thonicke et al. [2005], which uses PFT-specific emission factors from

Andreae and Merlet [2001] to convert fire carbon emissions to an ensemble of trace gases, including CO, CH₄, and NO_x.

The calculation of burned area in GlobFirm is based on a semiempirical approach taking into account the relationship between cumulative daily soil moisture and fire season length. Below a fuel-loading threshold, based on litter biomass, of 200 g C m⁻², fire is not possible; above this threshold, the probability of at least one fire in a day, $p(m)$, in a grid cell is estimated as

$$p(m) = e^{-\pi\left(\frac{m}{m_e}\right)^2} \quad (1)$$

where m_e is the moisture of extinction, which determines whether ignitions are possible if $m < m_e$. The grid cell average m_e is estimated as by using a weighted contribution, by litter biomass, of PFT-specific fuel flammability parameters, where the unweighted value is set to 0.3 for all PFTs for this study. The daily moisture status, m , estimated from the upper soil layer moisture (0–0.5 m depth), is used as an approximation for litter moisture. The length of the annual fire season (N) is estimated by summing the daily probability for fire, $p(m)$, over 365 days.

$$N = \sum_{n=1}^{365} p(m_n) \quad (2)$$

The annual fractional area burned is related to the length of the fire season (N) by a nonlinear empirical function calibrated with a global fire statistics database [Thonicke *et al.*, 2001]. Postfire mortality, defined as the number of individual trees killed, assumes 100% grass biomass and dead aboveground litter consumption and is calculated on an annual time step, with vegetation mortality and subsequent combustion efficiency linearly proportional to the grid cell burned area fraction scaled by PFT-specific fire resistances. Fire “resistance” is assumed to be higher for the tropical raingreen and temperate broadleaf evergreen PFTs (0.5) compared with the remaining woody PFTs (0.12).

In diagnostic mode, burned area is instead prescribed from satellite data with monthly frequency and with the prognostic burned area module disabled, and postfire mortality and trace gas emissions calculated on a monthly time step. To prepare the observed burned area data for model simulations, an initial prognostic LPJ-wsl fire simulation was conducted to create a monthly burned area time series beginning in 1901 and ending in 2009, modifying equation (2) to be called on a monthly rather than annual time step. Following the simulation, a correction factor was calculated, using the overlapping time period of the simulation with burned area data (see Table 1), as the monthly ratio between simulated and observed burned area climatology. The monthly correction factor was used to correct bias in the prognostic, presatellite era burned area. The corrected time series was merged with satellite-observed burned area to create a continuous 1901–2009 monthly burned area data set that was then used in the diagnostic simulations. This bias-correction step was important to more accurately represent the satellite-era fire regime during the historical simulation and to maintain a smooth transition in burned area between the simulated and the observed burned area data sets.

All model simulations were forced with monthly temperature, precipitation and cloud cover at 0.5° resolution obtained from the CRU TS3.1 data set for the years 1901–2009 [Mitchell and Jones, 2005]. A weather generator was used to disaggregate monthly climate data to daily values, with precipitation distributed randomly throughout the month according to number of wet days. Atmospheric CO₂ concentration [Keeling and Whorf, 2005] and soil texture from the Food and Agriculture Organization [Zobler, 1986] were prescribed, using a globally uniform soil depth of 1.5 m, where the upper soil layer is 0.5 m. Organic peatland soils are presently not represented in LPJ-wsl. A 1000 year spin up, which included fire from GlobFirm was implemented by recycling the first 30 years of climate data (1901–1930) and with fixed preindustrial CO₂ concentrations to equilibrate soil and vegetation carbon pools. After the spin up, a transient simulation beginning in 1901 and ending in 2009 was carried out with observed climate and CO₂ concentrations. For both the spin-up and transient simulations, only natural vegetation dynamics were simulated and land cover change and cropland dynamics were not included.

Five global simulations were run using LPJ-wsl including simulations with (1) no fire activity, (2) LPJ-wsl's prognostic fire module GlobFirm to estimate annual burned area, and (3–5) using LPJ-wsl with prescribed (or diagnostic) monthly burned area from the three satellite products: MODIS-GFED (3), L3JRC (4), and GlobCarbon (5).

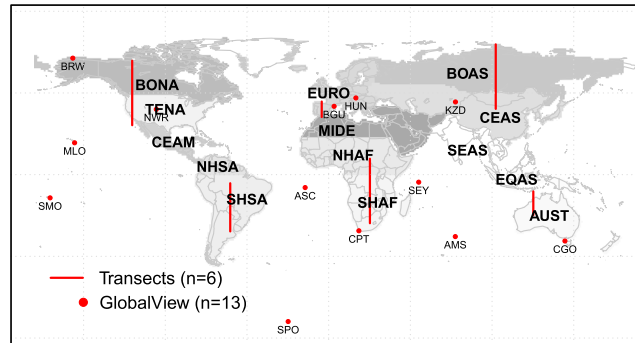


Figure 1. Global map showing the 14 GFED fire regions (in four letter, boldfaced code), the 13 GLOBALVIEW-CO/CO₂ observation stations (as three letter code), and the 6 continental transects.

2.3. Atmospheric Transport Modeling of CO₂ and CO

The off-line version (LMD_{zt}) of the general circulation model of the Laboratoire de Meteorologie Dynamique (LMD_z) [Hourdin and Armengaud, 1999] was used to transport CO₂ simulated by LPJ-wsl for 2000–2005. The air mass fluxes used in the off-line version were precalculated by the LMD_z online GCM nudged by ECMWF analysis of horizontal winds. The model has a horizontal resolution of 3.75° × 2.5° and 19 vertical levels. Monthly ocean and fossil fuel CO₂ fluxes were taken from the Takahashi

et al. [1999] ocean observations and the Edgar V4.1 fossil fuel database. LMD_{zt} calculates the CO₂ and CO concentrations at GlobalView observation stations and was driven by the monthly terrestrial CO₂ fluxes from LPJ-wsl net biome production (NBP, see equation (3)) and CO emissions estimated directly from the LPJ-wsl fire scenarios. Monthly net biome production was calculated as follows, where a negative value represents a flux into the atmosphere and positive values represent a terrestrial sink:

$$NBP = NPP - (R_h + F) \tag{3}$$

where *NPP* is net primary production (including carbon fluxes associated with seedling establishment), *R_h* is heterotrophic respiration, and *F* is the carbon flux from fire.

For CO transport, the Simplified Atmospheric Chemistry Assimilation System (SACS), coupled to LMD_{zt} was used to model chemical reactions between CO and OH that determine the lifetime of CO during the chemical transport process. SACS is a simplified version of the INCA model (INteraction Chimie Aérosols) [Folberth *et al.*, 2006] that consists in solving the chemical interaction between a limited set of four species, which represents the oxidation chain of methane: CH₄, HCHO, CO, and OH.

2.4. Model Benchmarking

Model simulations were compared to observations to rank model scenario performance for each of the prognostic or diagnostic burned area simulations considering vegetation (PFT) distributions, carbon stocks, and atmospheric CO and CO₂ concentrations. Model-data agreement was considered for six geographically representative latitudinal gradients, 14 GFED regions, and 13 NOAA GlobalView Observation Stations (Figure 1). The differences between model and observations (residuals) are presented here at the regional level using the 14 GFED regions that approximate major biomes and containing similar fire regimes.

PFT fractions and aboveground biomass from the five LPJ-wsl simulations were compared to observations as follows: (i) global tree cover fractions simulated by LPJ-wsl were calculated by summing the fractional coverage across all woody PFTs (for the averaging period 2000–2005) and compared to tree cover fractions from MODIS Collection 5 and GlobCover v2.2 PFT data sets from Poulter *et al.* [2011], and (ii) aboveground biomass, simulated by LPJ-wsl (the mean over 2000–2005), was scaled by 0.7 to remove the belowground biomass component and compared to a pantropical aboveground biomass data set [Saatchi *et al.*, 2011]. The pantropical biomass data set was developed by relating Lorey's tree height (the basal area weighted height of all trees > 10 cm in diameter) measured by the GLAS system onboard ICESAT, with regionally stratified height-biomass relationships. The original 1 km mean biomass data were aggregated to 0.5° resolution by applying a simple averaging window, and the variability within the 0.5° grid cell was calculated as the standard deviation of all 1 km observations.

Detrended monthly anomalies of observed and modeled CO and CO₂ concentrations were calculated at each station before goodness-of-fit statistics were estimated. Taylor diagrams [Taylor, 2001] were then used to visually assess the relative skill among model-data fit by comparing the linear correlation coefficient, root mean square difference, and the standard deviation in a polar coordinate plot. In addition, the mean-squared

Table 2. Global Summary of Simulated Carbon Fluxes (Pg C yr⁻¹) Carbon Stocks (Pg C) and Emissions From Fire (Pg C yr⁻¹) and Woody (Tree/Shrub) Vegetation Cover (Mkm²)^a

| LPJ-wsl Run | Annual NPP | Annual Rh | Total Biomass | Soil Carbon | C Emissions | CO Emissions | Woody Area | Vegetated Area (+Grassland) |
|-------------|------------|-----------|---------------|-------------|-------------|--------------|------------|-----------------------------|
| No fire | 58.8 | 56.3 | 814.4 | 1289.3 | — | — | 73.6 | 97.9 |
| Annual fire | 59.5 | 53.3 | 763.6 | 1226.8 | 3.65 | 0.70 | 70.0 | 97.7 |
| MODIS-GFED | 62.2 | 56.6 | 605.5 | 1283.3 | 3.03 | 0.58 | 62.8 | 97.7 |
| L3JRC | 62.7 | 55.8 | 571.6 | 1239.8 | 4.29 | 0.82 | 54.9 | 97.6 |
| GlobCarbon | 64.0 | 55.8 | 511.8 | 1227.1 | 5.60 | 1.08 | 59.2 | 97.7 |

^aMean from 1997 to 2006.

deviation (MSD) [Kobayashi and Salam, 2000] was used to quantitatively rank model performance. MSD is an integrated metric that describes the linear sum of the squared bias (SB), squared difference between model and observed standard deviations (SDSD), and the lack of correlation weighted by standard deviation (LCS), where SB is the difference between model (x) and observation means (y):

$$SB = (\bar{x} - \bar{y})^2 \quad (4)$$

The SDSD is difference between model (SD_m) and observation (SD_s) standard deviations, and a large value indicates that the model fails to simulate the amplitude of monthly fluctuations:

$$SDSD = (SD_s - SD_m)^2 \quad (5)$$

The LCS term reflects the lack of correlation (r) between observations and models and is weighted by standard deviations:

$$LCS = 2SD_sSD_m(1 - r) \quad (6)$$

Finally, MSD is the linear combination of (4)–(6):

$$MSD = SB + SDSD + LCS \quad (7)$$

3. Results

3.1. Summary of Global Fluxes and Stocks

At the global scale, differences between burned area scenarios led to predictable responses in changes of carbon fluxes and stocks as well as the total area of woody vegetation, both tree and shrubland (Table 2). Global average annual NPP was lowest for the no fire scenario (58.8 Pg C yr⁻¹), which also had the highest area of woody vegetation (73.6 million km²). In comparison, the global NPP for the scenarios that included fire ranged from 62.7 to 64.0 Pg C yr⁻¹ and also had a lower area of woody vegetation (54.9–70.1 Mkm²) and a higher area of more productive grasslands (Table 2). For the five scenarios considered, global aboveground and belowground live biomass ranged from 511 to 814 Pg C and was highest for the no fire scenario by 60–300 Pg C. Mineral soil carbon was also higher for the no fire scenario but by a smaller amount (5–60 Pg C) relative to the total soil carbon pool (~1250 Pg C). Heterotrophic respiration was generally higher for the scenario with no fire (56.3 Pg C yr⁻¹) in comparison to scenarios that included fire (53.3–56.6 Pg C yr⁻¹), with the MODIS-GFED burned area scenario having higher global R_h (55.8 Pg C yr⁻¹) in the topical forested regions of SHSA and EQAS (in Figure 1). Global carbon and CO emissions from combustion during fire ranged from 3.0 to 5.6 Pg C yr⁻¹ and 0.7 to 1.08 Pg CO yr⁻¹, respectively. Net biome production (equation (3) and using the values from Table 2) was 2.50 Pg C yr⁻¹, with the positive value indicating a carbon sink, for the no fire scenario and surprisingly similar across all the fire scenarios, ranging from 2.55 to 2.61 Pg C yr⁻¹. All key global carbon and forest area metrics were within the range of known values and their uncertainties for biomass [Pan et al., 2011], soils [Davidson and Janssens, 2006], NPP and R_h [Zhao and Running, 2010], C and CO emissions [Andreae and Merlet, 2001], and tree cover [Hansen et al., 2010].

Annual global burned area ranged from 1.4 to 3.8 Mkm² yr⁻¹ (Table 2 and Figure 2), with the LPJ-wsl prognostic simulation, using the GlobFirm module, underestimating fire in all but the most mesic biomes compared to the observed burned area data sets (Figure 3). Among the satellite products, the largest differences for the magnitude of burned area were found in boreal regions (i.e., BONA and BOAS; Figure 3), where MODIS-GFED estimated significantly lower burned area (0.069 Mkm² yr⁻¹ for Boreal Asia) compared with

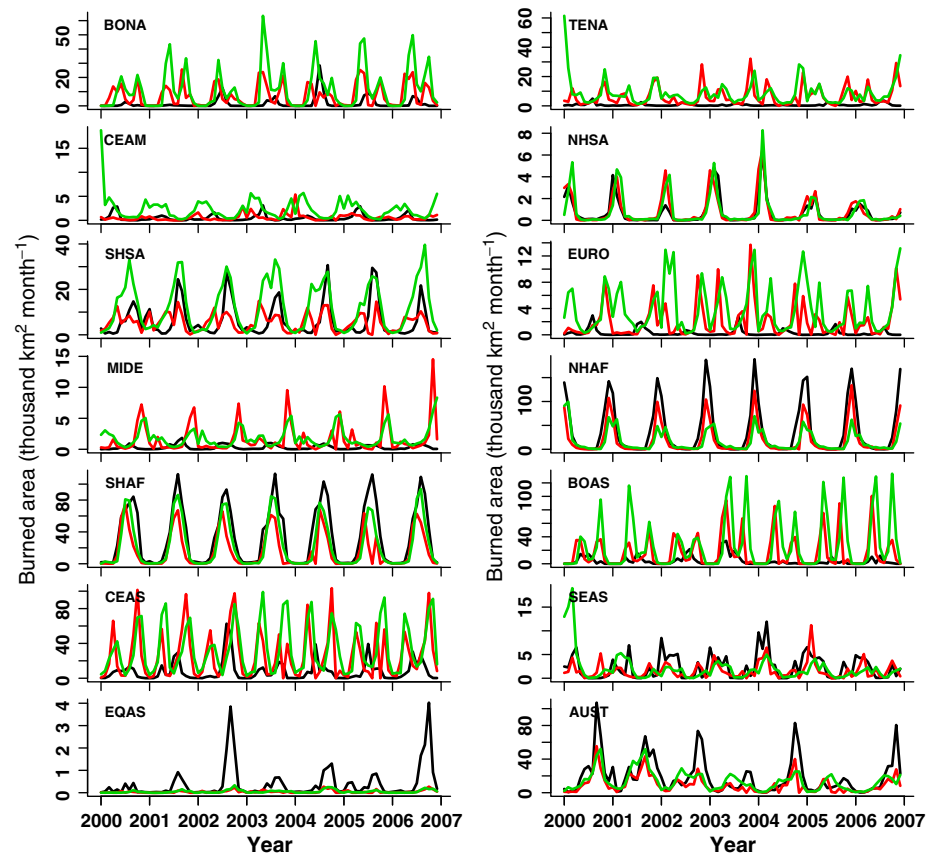


Figure 2. Monthly burned area by GFED region (see Figure 1) for each of the three observed satellite products (GFED = black line, GlobCarbon = red line, L3JRC = green line).

L3JRC ($0.42 \text{ Mkm}^2 \text{ yr}^{-1}$) and GlobCarbon ($0.27 \text{ Mkm}^2 \text{ yr}^{-1}$). High burned area variability was also observed in savanna regions, especially across Africa (SHAF), where the MODIS-GFED estimate of $2.5 \text{ Mkm}^2 \text{ yr}^{-1}$ was almost double that of L3JRC ($1.4 \text{ Mkm}^2 \text{ yr}^{-1}$) and GlobCarbon ($1.2 \text{ Mkm}^2 \text{ yr}^{-1}$) (Figure 2 and Table S1). The difference in boreal burned area was due to a combination of L3JRC overestimating fire (i.e., positive bias), particularly in extreme years (Figure 2), and MODIS-GFED most likely underestimating fire in comparison to reference ground-based data [Chang and Song, 2009; Kasischke et al., 2011]. In Africa, MODIS burned area, using the algorithm of Roy et al. [2005], was found to be more accurate than L3JRC and an “unfiltered” version of the GlobCarbon product used in this study across a range of grassland and savanna systems using Landsat as a reference for burned area [Roy and Boschetti, 2009]. In the wet tropics (i.e., the GFED regions of CEAM, SEAS, and EQAS), the satellite data were more consistent with one another (Table S1), but the LPJ-wsl prognostic simulation generally estimated an annual burned area that was too high in both the Amazon and Congo Basins (Figure 3). Differences among burned area data sets have not yet been extensively addressed for the tropics in comparison to temperate and boreal regions due to a lack of observational data, but it is suspected that remotely sensed burned area underestimates tropical fires because of cloud cover problems and because tropical-deforestation fires can be small in size [Giglio et al., 2006]. Across all regions, interannual variability in burned area showed greatest agreement for the savanna regions, where the area burned was much larger, and as total area burned decreased at the regional level, agreement in interannual variability also decreased (Figure 3).

3.2. Regional Vegetation and Biomass Patterns

Regional sensitivity of vegetation cover and biomass to fire also followed predictable covariation in ecosystem processes with burned area. The savanna regions (SHSA, NHAF, and SHAF) accounted for the 44–73% of global burned area (Table S1) and about 20–30% of the area of woody vegetation (Table S2), while boreal regions (BONA and BOAS) contributed to 2.4–14% of global burned area, containing about 24% of global woody vegetation. For the control scenario with no fire, tree cover and biomass were highest across all regions

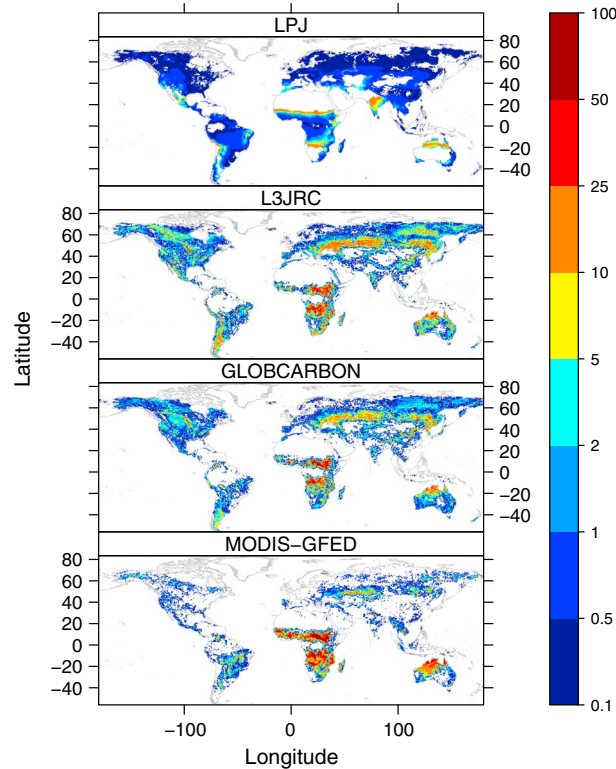


Figure 3. Average annual grid cell fraction burned for the three observed satellite products and the LPJ-wsl annual fire simulations calculated from burned area data over the years 1999–2006 where a common overlap between satellite data exists.

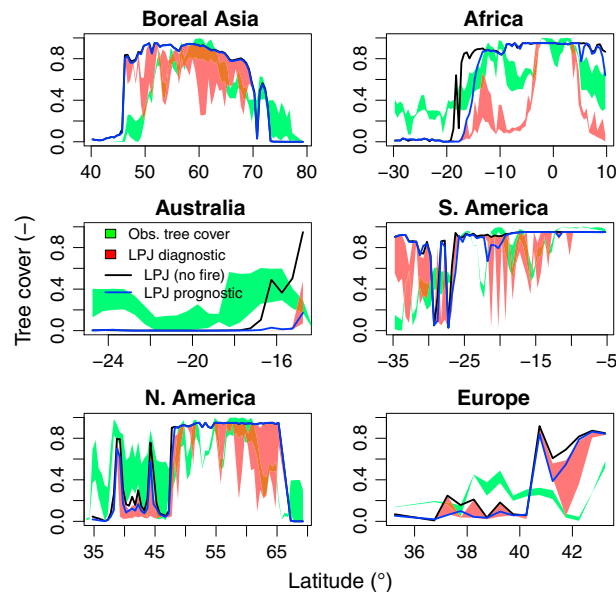


Figure 4. Simulated tree cover fraction for all five-model runs (three satellite driven estimates are shown displayed in “LPJ-wsl diagnostic”) along each of the six transects (Figure 1) in comparison with observed tree cover (from MODIS-GFED and GlobCover land cover products).

(Table S2), with the variability in the degree of regional sensitivity to fire explained by climate limitations i.e., dry regions with low biomass or regions with high precipitation.

At the scale of the latitudinal transects, differences between burned area scenarios provided insight for generating hypotheses that could explain the residual between simulated and observed tree cover. Because the prognostic fire model generally underestimated burned area, the largest differences in comparison to observed burned area were found in Africa and Australia, where satellite burned area was greatest (Figure 4). In the moderately fire dependent biomes, North and South America and Boreal Asia, the differences in simulated and observed burned area were less noticeable (Figure S1). Along each transect, simulated tree cover had large responses to observed burned area, especially in Africa where the modeled response of vegetation to observed fire was too sensitive in comparison to observations of tree cover (Figure 4). Both the no fire and prognostic fire scenarios tended to overestimate biomass in the African savanna regions (Figure 5), with fire reducing potential biomass from 57 Mg C ha⁻¹ to 20–27 Mg C ha⁻¹ in the savanna biome (Table S3; i.e., SHAF and NHAF). The response of tree cover to fire in Australia revealed a pattern where simulated woody vegetation was largely climate limited, suggesting that including a drought tolerant PFT may improve model performance, but conversely, the biomass from the *Saatchi et al.* [2011] data set may be overestimated in these dryland regions [Mitchard et al., 2013].

Along the boreal transect, the diagnostic fire simulations did not significantly improve the limits of southern and northern tree line, suggesting that bioclimatic thresholds or belowground processes, such as permafrost, which is not included in LPJ-wsl, are limiting forest distribution rather than disturbance [Beer et al., 2007]. In South America, known land-use interactions with deforestation and fire create complex spatial patterns in tree cover (Figures 4 and 5) and thus using actual land cover in the LPJ-wsl simulations would be expected to improve the modeled biomass gradient.

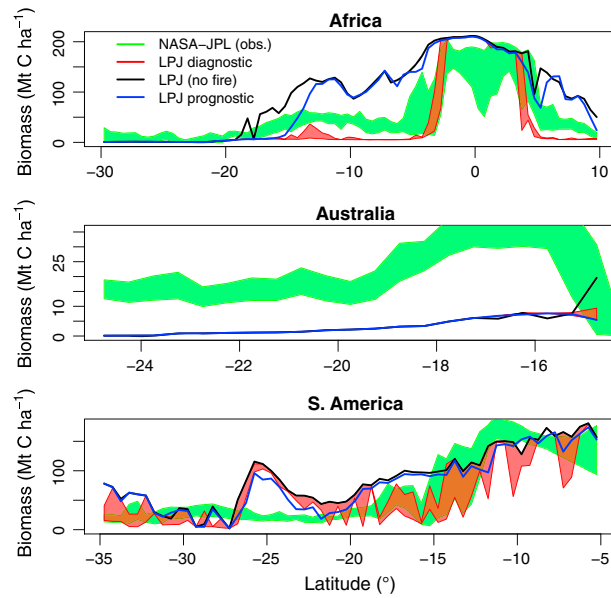


Figure 5. Tropical aboveground biomass estimates for the three tropical transects (Figure 1) using the NASA-JPL biomass estimates as a benchmark.

Finally, most North American and European landscapes have been heavily influenced by conversion of forests to agriculture, with fire being strictly managed or suppressed, making prognostic fire simulations challenging. Nevertheless, we found that satellite burned area improved tree line in boreal Canada and northern Spain, but that simulated tree cover was too low in the Mediterranean region, confirming some combination of the same model or data bias limiting woody vegetation growth in dry climates as found in the Australia transect and possibly overly sensitive PFT traits to fire (Figure 4). Overall, MODIS-GFED burned area generated highest model-data agreement in the tropical forest regions (Table 3), whereas L3JRC burned area had higher agreement in temperate and boreal regions. No observed burned area product was able to consistently and accurately inform LPJ-wsl to reproduce savanna vegetation (Table 3), either because savanna

burned area was overestimated or because the LPJ plant functional types were too broadly defined to include fire adapted species.

3.3. Trace Gas Transport CO and CO₂

CO and CO₂ concentrations represent contrasting biogeochemical tracers that are emitted as fuels are consumed by fire and are both useful indicators in assessing model ability to estimate emissions and vegetation regrowth. Apart from minor anthropogenic and oceanic sources, global CO observations are driven mainly from fire [Pison *et al.*, 2009], whereas station CO₂ concentrations and anomalies are composed of a mixture of fire emissions as well feedbacks from the net balance of photosynthesis and ecosystem respiration. As such, CO could be expected to provide a more direct benchmark with which to evaluate burned area and subsequent emission, whereas in contrast, CO₂ provides an integrated ecosystem response.

Results from the atmospheric transport modeling clearly distinguished the utility in using CO versus CO₂ fluxes to evaluate burned area and vegetation interactions. We observed high variability across the

Table 3. Model Simulation That Resulted in the Lowest Regional Residual or Bias Between Observations and Model Variable (See Figure 1 for Locations)

| Full Name | Acronym | Tree Cover | Mean Biomass |
|-----------------------------------|---------|------------|-------------------|
| Boreal North America | BONA | L3JRC | No data available |
| Temperate North America | TENA | L3JRC | GlobCarbon |
| Central America | CEAM | Prognostic | L3JRC |
| Northern Hemisphere South America | NHSA | L3JRC | Prognostic |
| Southern Hemisphere South America | SHSA | L3JRC | GlobCarbon |
| Europe | EURO | L3JRC | No data available |
| Middle East | MIDE | No fire | No fire |
| Northern Hemisphere Africa | NHAF | Prognostic | Prognostic |
| Southern Hemisphere Africa | SHAF | Prognostic | GlobCarbon |
| Boreal Asia | BOAS | GlobCarbon | No data available |
| Central Asia | CEAS | L3JRC | No fire |
| Southeast Asia | SEAS | GFED | No fire |
| Equatorial Asia | EQAS | GFED | GFED |
| Australia and New Zealand | AUST | No fire | No fire |

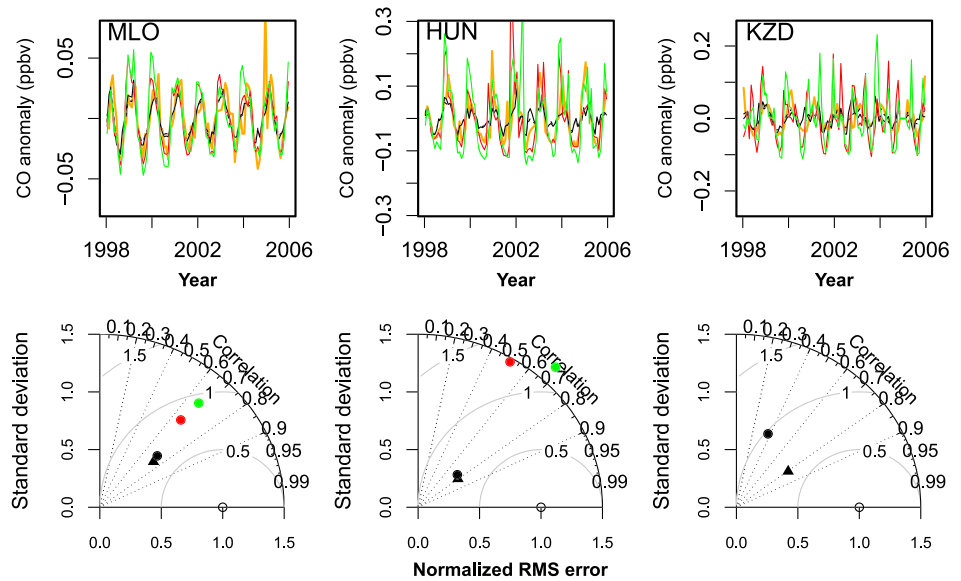


Figure 6. (top) Detrended monthly anomalies for CO at three stations (indicated in Figure 1). The observations are in orange, the MODIS-GFED scenario in black, L3JRC in red, and GlobCarbon in green. (bottom) Taylor diagrams that illustrate several goodness-of-fit criteria (as discussed in main text). For KZD, the L3JRC and GlobCarbon points are not included on the plot because their standard deviations are greater than 1.5.

different burned area scenarios that were recorded by the CO emissions (Figure 6) and lower variability in CO₂ emissions (Figure 7). The highest CO and CO₂ fluxes were observed in the savanna regions of South America and Africa (Table S4), where burned area was also largest. Our simulated CO emissions using MODIS-GFED burned area produced the closest agreement with observed CO for the majority of stations, where high agreement is shown by the highest Taylor skill and the lowest MSD (Table 4). The MSD statistic was mainly influenced by the contribution of the SDSA term, indicating that mismatches in amplitude were the main cause for the differences between observation and modeled CO as opposed to error from bias and correlations. The independent GFED CO emissions, simulated using the CASA model from

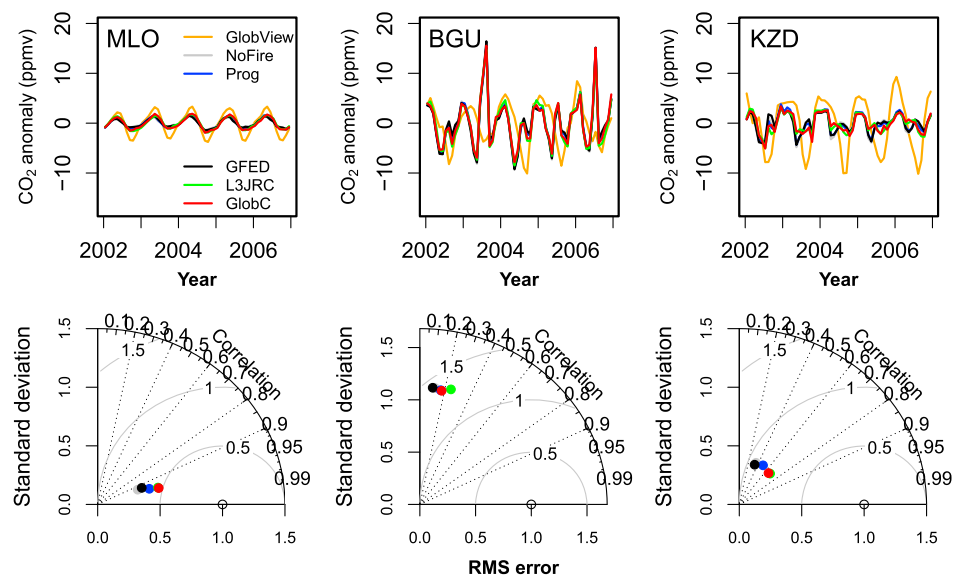


Figure 7. (top) Detrended monthly anomalies for CO₂ at three stations (indicated in Figure 1). The observations are in orange, the MODIS-GFED scenario in black, L3JRC in red, and GlobCarbon in green. (bottom) Taylor diagrams that illustrate several goodness-of-fit criteria (as discussed in main text).

Table 4. Model Simulation That Resulted in the Lowest MSD Statistic at Each GlobalView Observation Station (See Figure 1 for Locations)

| GlobalView Site Name | Transport of CO | Transport of CO ₂ |
|----------------------|-----------------|------------------------------|
| KZD | GFED | GlobCarbon |
| CGO | GlobCarbon | L3JRC |
| BGU | No data | L3JRC |
| MLO | GFED | GlobCarbon |
| HUN | GFED | No data |
| NWR | GFED | GlobCarbon |
| BRW | GFED | GlobCarbon |
| CPT | No data | L3JRC |
| ASC | GFED | Prognostic |
| SEY | L3JRC | GFED |
| SPO | GFED | L3JRC |
| SMO | GFED | GFED |
| AMS | No data | GFED |

less well, with amplitudes that were too large (i.e., ratio of standard deviations > 1; Figure 6, bottom) and slightly lower R^2 than at MLO.

The CO₂ signal was much less variable between the no fire and ensemble of fire simulations compared with the CO signal (Figure 7). At MLO, a high correlation ($R^2 > \sim 0.9$) was found for all simulations, but at BGU, the model-data agreement was noticeably lower ($R^2 < \sim 0.25$). Importantly, all scenarios that included fire showed improvements over the scenario with no fire, with improvements (shown in the Figure 7 Taylor diagrams) in both the correlation (seasonality) and in amplitudes (difference between winter maxima and summer minima). In contrast to CO, we found that there was no burned area product able to produce consistently high-scores between the model and the global observation tower network. GlobCarbon had the lowest MSD for the northern latitude stations (KZD, MLO, NWR, BRW) and GFED or L3JRC performed better for the southern Hemisphere stations. At MLO, the ratio of the standard deviations was especially low (Figure 7) despite a relatively high correlation with observations. Burned area did not improve amplitude at MLO but did reduce the bias and slightly improved the correlations with the GlobCarbon burned area ($R^2 \sim 0.9$). At BGU, the amplitude (ratio of standard deviations) was closer to 1 for all simulations, but this site had low correlations. KZD measured similarly to MLO, with reasonable R^2 values between 0.4 and 0.6, but with seasonal amplitude too low, i.e., low ratio of standard deviations, that contributed to a systematic bias compared to observations.

4. Discussion

4.1. Toward Comprehensive Monitoring of Fire Trends in the Earth System

The role of fire in the terrestrial biosphere has long been recognized as a critical process influencing biogeography, biogeochemistry, and biophysics of the land surface [Bowman *et al.*, 2009; Marlon *et al.*, 2008; Randerson *et al.*, 2006]. At global scales, a wealth of empirical studies have documented the global importance of fire on interannual variability of atmospheric CO₂ concentrations and in determining the boundaries of ecosystem types and their biophysical properties. While global carbon cycle research has made several recent advances in the modeling of fire processes [Hessl, 2011], only a subset of models consistently includes fire as a disturbance as shown in a series of major syntheses on the carbon cycle (e.g., the CMIP5 Earth system model intercomparison [Anav *et al.*, 2013], the TRENDY intermodel comparison [Sitch *et al.*, 2013], and the North American Carbon Program Regional Synthesis and MsTMIP [Fisher *et al.*, 2014; Huntzinger *et al.*, 2013, 2012]). As our study has shown, the dynamic representation of fire in global carbon cycle models is critical for establishing realistic initial conditions for tree cover and carbon stocks as shaped by disturbance regimes, which then determine the system response to interannual climate variability and long-term sensitivity to climate (i.e., “gamma”) [Piao *et al.*, 2013].

At short, interannual timescales, the putative role of fire as a driver of atmospheric CO₂ growth rate anomalies has recently been called into question by Prentice *et al.* [2011]. The authors argued that this correlation may be an artifact of increased human activities related to burning that are more common during drought years, especially in Southeast Asia, where subsequent peat fires, with “high-density” carbon

van der Werf et al. [2003], were quite similar to the LPJ-wsl simulated CO emissions, suggesting similarity between the initial conditions for biomass and/or the combustion fractions between CASA and the LPJ models. At Mauna Loa (MLO), the correlations were similar between diagnostic simulations and the observations for CO ($R^2 = 0.6\text{--}0.8$), which indicated that the seasonality of burned area was similar, but the amplitudes varied (Figure 6, top). At HUN and KZD, the L3JRC and GlobCarbon simulations performed

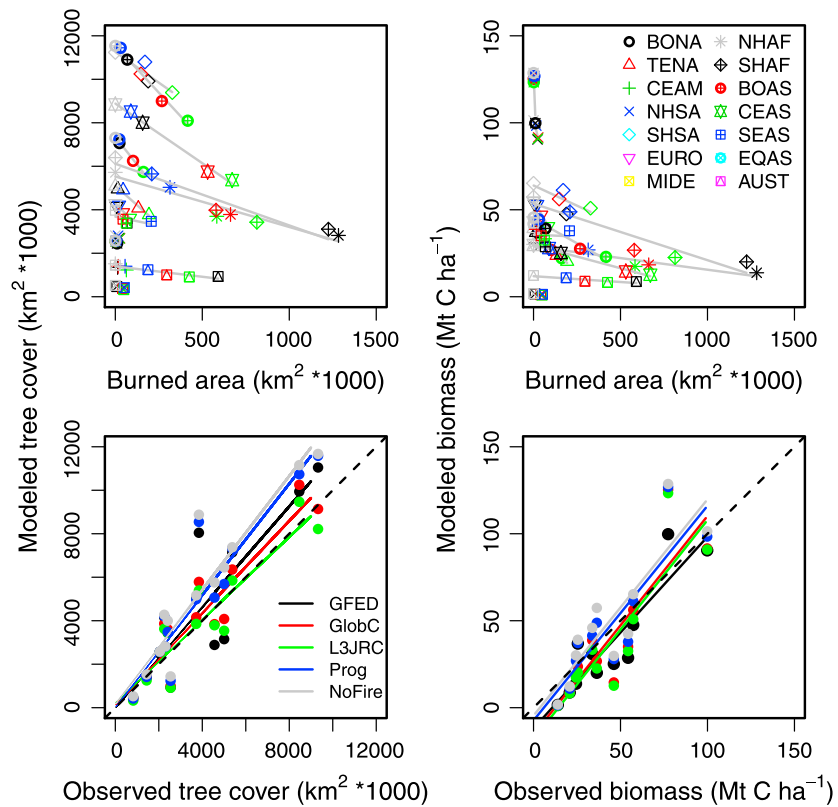


Figure 8. (top) Sensitivity of tree cover and biomass to burned area for each of the GFED regions. (bottom) Improvement in simulated tree cover and biomass for each model X fire simulation, with individual points being the GFED regions.

emissions, dominated emissions in the 1997–1998 ENSO. Our findings provide support to the idea that burned area variability does not directly translate to large CO₂ emission anomalies at global scales, where we find NBP to be relatively robust to differences in burned area via compensation by ecosystem respiration. In addition, at subannual scales, we found that differences in atmospheric CO₂ concentrations at observation stations (Figure 7) were relatively minor among fire scenarios and even in comparison to the “no fire” scenario. These small differences point toward inherent carbon turnover rates driven by heterotrophic respiration, especially in grassland areas, which continue to drive carbon losses even when fire is suppressed. These compensatory mechanisms vary between models, however, where in contrast the CLM4.5 DGVM, *Li et al.* [2013] observed that fire caused global NBP to decrease in sink strength by ~1.0 Pg C yr⁻¹, due to reductions in global NPP, whereas the increase in grassland area simulated by LPJ-wsl led to greater global NPP.

The emissions of non-CO₂ gases were shown to be important as a model benchmark, as demonstrated from our analysis of CO. The emissions of CO, as well as CH₄, also emitted during fires, reduce the concentrations of OH in the atmosphere as it is oxidized [*Hauglustaine et al.*, 1999]. This change in atmospheric OH chemistry then has important implications for the sink dynamics of additional reactive greenhouse gases, especially methane [*Bousquet et al.*, 2006]. The inclusion of prognostic peat fires and smoldering fires that generate high CO emissions from incomplete combustion would contribute to improved model-data performance compared with the GlobalView monitoring station network.

4.2. Key Sensitivities and Feedbacks to Prioritize Model Development

To diagnose large-scale sensitivities between tree cover, biomass, and fire, we estimated empirical statistical relationships for each GFED region (Figure 8). The feedbacks from burned area on tree cover and biomass were strongly linear but with different sensitivities, where the slopes of the linear model were strongly biome dependent (Figure 8, top). Except for the tropical wet biomes (SEAS and CEAM) and the driest biomes (MIDE and AUST), where fire is either climate or fuel limited, a simple linear regression model of tree cover and

burned area was sufficient to explain >80% of the variability in tree cover. The most sensitive regions to fire variability were the temperate and boreal regions (a 7–10% decrease in tree cover for a 1000 km² increase in burned area, $P < 0.005$). Modeled biomass also followed a similar, linear response to burned area, with a decrease of about 0.1 Mg C ha⁻¹ per 1000 km² increase in fire in the northern biomes.

Compared with the prognostic fire scenario, all three satellite products improve the model-data fit between burned area, tree cover, and biomass by reducing bias, particularly in the regions where climate is able to support continuous forest area (Figure 8, bottom). In the regions where litter biomass loads are lower (i.e., grasslands and savannas), the sensitivity of fixed thresholds related to fuel loading and the maintenance of fire become more important, e.g., 200 g C m⁻² in the Glob-FIRM model or 50 Kw m⁻² in SPITFIRE [Thonicke *et al.*, 2010], and should be considered in more detail. For example, subpixel variation in fuel loading may be sufficient to allow fire to spread, but at larger spatial scales, this assumption may generalize “clumping” features of fuel distributions that may allow fire to occur. In addition, the representation of savanna vegetation in the presence of the fire return interval from observations requires consideration of the resilience of savanna vegetation to fire, which may be underestimated in LPJ, the diversity of plant strategies including the consideration of shrub PFTs that are adapted to frequent fires [Higgins *et al.*, 2012].

Interactions between fire and land use are perhaps equally important for initializing model simulations as parameters for describing fire effects. The inclusion of land use in our model simulations would lead to improved biomass estimation, especially along the tropical transects where forest conversion to pasture and cropland has taken place. Land use can also serve as an important source of ignition from land clearing activities [Pfeffer *et al.*, 2013; Poulter *et al.*, 2010] and is likely a more clear cause of ignitions than population density, currently used in SPITFIRE. For example, the partitioning of fire emissions from natural and small agricultural fires has recently been recognized as increasing global burned area and emissions by 20–30% [Randerson *et al.*, 2012]. However, reductions in land-use intensity resulting from abandonment can reduce ignitions but also lead to larger fires from reduced fire management and suppression.

4.3. Data Needs for Model Optimization and Assimilation

Expanded monitoring of burned area from space is needed to improve, develop, and benchmark new fire models. In particular, information on burned area, fire duration, and intensity, including observation uncertainties, is required to parameterize fire spread and fire severity models. Key parameters from field studies required for model optimization include thresholds related to biomass and moisture that determine the duration, spread, and intensity of fire. The testing of model structure, by implementing a variety of fire spread models and fire danger indices, is also a useful method for identifying where global assumptions may mismatch with regional processes [Keane *et al.*, 2004]. Satellite data on greenhouse gas emissions estimated from fire radiative power [Kaiser *et al.*, 2012] can also be used in inversion models to estimate point sources and also contribute to land surface model calibration, yet the diurnal cycle of fire intensity requires high-temporal observations. At the site level, field observations of postfire forest mortality [Murphy *et al.*, 2010], including the short-term and long-term plant responses [Varner *et al.*, 2009], to fire intensity are required for a range of biomes to assist in calibrating fire effects. Fire intensity is particularly important because it determines combustion efficiencies and the amount of biomass oxidized during fire.

Reducing and attributing the uncertainties between different satellite products is necessary for guiding modeling community efforts in understanding fire dynamics. For example, the three different products used here to provide burned area are known to not perform consistently from biome to biome, with MODIS-GFED providing estimates more closely related to observations in temperate and boreal regions [Kasischke *et al.*, 2011] yet possibly overestimating savanna fires compared with L3JRC and GlobCarbon [Giglio *et al.*, 2006, 2010]. Our model evaluation provides further support that GFED burned area may be superior in the higher latitudes, based on a range of metrics; however, the burned area differences in the savannas provide no clear answer as to which product performs most closely to observations. The release of GFEDv4.0 adds additional discrepancies among existing burned area data sources, because of the inclusion of small fires from agriculture [Randerson *et al.*, 2012]. Further burned area product development, such as ongoing work in European Space Agency (ESA) Climate Change Initiative, is required to fulfill these needs [Mouillot *et al.*, 2014]. The ESA led “fire_cci” initiative expects to address these issues by providing the global modeling community with a consistent series of burned area, and its uncertainty, using regionally trained algorithms to map fire scars at moderate spatial resolution.

5. Conclusion

Future carbon cycle model development will continue to represent the effects of fire on the carbon cycle and the feedbacks of fire on vegetation and fuel loading. The new generation of process-based fire modeling frameworks, where ignitions, fire behavior, fire effects, and the estimation of trace gas emissions are individually considered, provides many opportunities for model improvement over semiempirical approaches. However, carbon cycle models exhibit large sensitivity to variations in burned area, as shown in our study with LPJ, and thus consideration to observed burned area uncertainty is essential. As improved detection algorithms are integrated with fire remote sensing systems, large gains can be expected in model development and benchmarking helping to establish improved initial conditions within Earth system models.

Acknowledgments

B. P. acknowledges funding from an FP7 Marie Curie Incoming International Fellowship (grant 220546). This study was partly supported by the fire_cci project (<http://www.esa-fire-cci.org/>), funded by the European Space Agency. The climate, land cover, and burned area data sets used in this study are available at <http://badc.nerc.ac.uk/data/cru/>, <http://poulterlab.com/datasets/> and <http://www.globalfiredata.org/>. We appreciate the constructive feedback from three anonymous reviewers that greatly improved the discussion on integrating burned area data within process-based models.

References

- Anav, A., P. Friedlingstein, M. Kidston, L. Bopp, P. Ciais, P. Cox, C. Jones, M. Jung, R. Myrneni, and Z. Zhu (2013), Evaluating the land and ocean components of the global carbon cycle in the CMIP5 earth system models, *J. Clim.*, *26*, 6801–6843, doi:10.1175/JCLI-D-12-00417.1.
- Andreae, M. O., and P. Merlet (2001), Emission of trace gases and aerosols from biomass burning, *Global Biogeochem. Cycles*, *15*(4), 955–996, doi:10.1029/2000GB001382.
- Aragão, L. E. O. C., Y. Malhi, N. Barbier, A. Lima, Y. Shimabukuro, L. O. Anderson, and S. S. Saatchi (2008), Interactions between rainfall, deforestation and fires during recent years in the Brazilian Amazonia, *Philos. Trans. R. Soc. London, Ser. B*, *363*, 1779–1785.
- Archibald, S., C. E. R. Lehmann, J. L. Gomez-Dans, and R. A. Bradstock (2013), Defining pyromes and global syndromes of fire regimes, *Proc. Natl. Acad. Sci. U.S.A.*, *110*(16), 6442–6447, doi:10.1073/pnas.1211466110.
- Arino, O., S. Casadio, and D. Serpe (2011), Global night-time fire season timing and fire count trends using the ATSR instrument series, *Remote Sens. Environ.*, *116*, 226–238.
- Arora, V. K., and G. J. Boer (2005), Fire as an interactive component of dynamic vegetation models, *J. Geophys. Res.*, *110*, G02008, doi:10.1029/2005JG000042.
- Bachelet, D., J. M. Lenihan, C. Daly, and R. P. Neilson (2000), Interactions between fire, grazing and climate change at Wind Cave National Park, SD, *Ecol. Modell.*, *134*, 229–244.
- Beer, C., W. Lucht, D. Gerten, K. Thonicke, and C. Schimmlus (2007), Effects of soil freezing and thawing on vegetation carbon density in Siberia—A modeling analysis with the LPJ-DGVM, *Global Biogeochem. Cycles*, *21*, GB1012, doi:10.1029/2006GB002760.
- Bond, W. J., and J. E. Keely (2005), Fire as a global 'herbivore': The ecology and evolution of flammable ecosystems, *Trends Ecol. Evol.*, *20*(7), 387–394.
- Bond, W. J., F. I. Woodward, and G. F. Midgley (2005), The global distribution of ecosystems in a world without fire, *New Phytol.*, *165*, 525–538.
- Bousquet, P., et al. (2006), Contribution of anthropogenic and natural sources to atmospheric methane variability, *Nature*, *443*(28), 439–443.
- Bowman, D. M. J. S., et al. (2009), Fire in the earth system, *Science*, *324*, 481–484.
- Chang, D., and Y. Song (2009), Comparison of L3JRC and MODIS global burned area products, *J. Geophys. Res.*, *114*, D16106, doi:10.1029/2008JD011361.
- Ciais, P., et al. (2013), Current systematic carbon cycle observations and needs for implementing a policy-relevant carbon observing system, *Biogeosci. Discuss.*, *10*(7), 11,447–11,581.
- Costa, L., K. Thonicke, B. Poulter, and F. W. Badeck (2011), Climate and human drivers of fires in Portugal, *Reg. Environ. Change*, *11*(3), 543–551.
- Davidson, E. A., and I. A. Janssens (2006), Temperature sensitivity of soil carbon decomposition and feedbacks to climate change, *Nature*, *440*, 165–173, doi:10.1038/nature04514.
- Fisher, J. B., et al. (2014), Carbon cycle uncertainty in the Alaskan Arctic, *Biogeosciences*, *11*(15), 4271–4288.
- Folberth, G. A., D. A. Hauglustaine, J. Lathiere, and F. Brocheton (2006), Interactive chemistry in the Laboratoire de Météorologie Dynamique general circulation model: Model description and impact analysis of biogenic hydrocarbons on tropospheric chemistry, *Atmos. Chem. Phys.*, *6*, 2273–2319.
- Gerten, D., S. Schaphoff, U. Haberlandt, W. Lucht, and S. Sitch (2004), Terrestrial vegetation and water balance—Hydrological evaluation of a dynamic global vegetation model, *J. Hydrol.*, *286*, 249–270.
- Giglio, L., I. Csizsar, and C. O. Justice (2006), Global distribution and seasonality of active fires as observed with the Terra and Aqua Moderate Resolution Imaging Spectroradiometer (MODIS) sensors, *J. Geophys. Res.*, *111*, G02016, doi:10.1029/2005JG000142.
- Giglio, L., T. Loboda, D. P. Roy, B. Quayle, and C. O. Justice (2009), An active-fire based burned area mapping algorithm for the MODIS sensor, *Remote Sens. Environ.*, *113*, 408–420.
- Giglio, L., J. T. Randerson, G. R. van der Werf, P. S. Kasibhatla, G. J. Collatz, D. C. Morton, and R. S. DeFries (2010), Assessing variability and long-term trends in burned area by merging multiple satellite fire products, *Biogeosciences*, *7*, 1171–1186.
- Hansen, M., S. V. Stehman, and P. V. Potapov (2010), Quantification of global gross forest cover loss, *Proc. Natl. Acad. Sci. U.S.A.*, *107*(19), 8650–8655, doi:10.1073/pnas.0912668107.
- Hauglustaine, D. A., G. P. Brasseur, and J. S. Levine (1999), A sensitivity simulation of tropospheric ozone changes due to the 1997 Indonesian fire emissions, *Geophys. Res. Lett.*, *26*(21), 3305–3308, doi:10.1029/1999GL900610.
- Hessl, A. E. (2011), Pathways for climate change effects on fire: Models, data, and uncertainties, *Prog. Phys. Geogr.*, *35*(3), 393–407.
- Higgins, S. I., W. J. Bond, H. Combrink, J. M. Craine, E. C. February, N. Govender, K. Lannas, G. Moncreif, and W. Trollope (2012), Which traits determine shifts in the abundance of tree species in a fire-prone savanna?, *J. Ecol.*, *100*, 1400–1410.
- Hourdin, F., and A. Armengaud (1999), The use of finite-volume methods for atmospheric advection of trace species. Part I: Test of various formulations in a general circulation model, *Mon. Weather Rev.*, *127*, 822–837.
- Huntzinger, D. N., et al. (2012), North American Carbon Program (NACP) regional interim synthesis: Terrestrial biospheric model intercomparison, *Ecol. Modell.*, *232*, 144–157.
- Huntzinger, D. N., et al. (2013), The North American Carbon Program Multi-Scale Synthesis and Terrestrial Model Intercomparison Project—Part 1: Overview and experimental design, *Geosci. Model Dev.*, *6*(6), 2121–2133.
- Kaiser, J. W., et al. (2012), Biomass burning emissions estimated with a global fire assimilation system based on observed fire radiative power, *Biogeosciences*, *9*, 527–554.

- Kasischke, E. S., T. Loboda, L. Giglio, N. H. F. French, E. E. Hoy, B. de Jong, and D. Riano (2011), Quantifying burned area for North American forests: Implications for direct reduction of carbon stocks, *J. Geophys. Res.*, *116*, G04003, doi:10.1029/2011JG001707.
- Keane, R. E., G. J. Cary, I. D. Davies, M. D. Flannigan, R. H. Gardner, S. Lavorel, J. M. Lenihan, C. Li, and T. S. Rupp (2004), A classification of landscape fire succession models: Spatial simulations of fire and vegetation dynamics, *Ecol. Modell.*, *179*, 3–27.
- Keeling, C. D., and T. Whorf (2005), Atmospheric CO₂ records from sites in the SIO air sampling network, *Rep.*, Carbon Dioxide Information Analysis Center, Oak Ridge National Laboratory, Oak Ridge, Tenn.
- Kloster, S., N. M. Mahowald, J. Randerson, P. E. Thornton, F. M. Hoffman, S. Levis, P. J. Lawrence, J. J. Feddes, K. Oleson, and D. M. Lawrence (2010), Fire dynamics during the 20th century simulated by the Community Land Model, *Biogeosciences*, *7*, 565–630.
- Knorr, W., V. Lehsten, and A. Arneft (2012), Determinants and predictability of global wildfire emissions, *Atmos. Chem. Phys.*, *12*, 6845–6861.
- Kobayashi, K., and M. U. Salam (2000), Comparing simulated and measured values using mean squared deviation and its components, *Agron. J.*, *92*, 345–352.
- Krause, A., S. Kloster, S. Wilkenskjaeld, and H. Paeth (2014), The sensitivity of global wildfires to simulated past, present and future lightning frequency, *J. Geophys. Res. Biogeosci.*, *119*, 312–322, doi:10.1002/2013JG002502.
- Langenfelds, R. L., R. J. Francey, B. Pak, L. P. Steele, J. Lloyd, C. M. Trudinger, and C. E. Allison (2002), Interannual growth rate variations of atmospheric CO₂ and its δ¹³C, H₂, CH₄, and CO between 1992 and 1999 linked to biomass burning, *Global Biogeochem. Cycles*, *16*(3), 1048, doi:10.1029/2001GB001466.
- Lehsten, V., K. J. Tansey, H. Balzer, K. Thonicke, A. Spessa, U. Weber, B. Smith, and A. Arneft (2008), Estimating carbon emissions from African wildfires, *Biogeosciences*, *6*, 349–360.
- Li, F., X. D. Zeng, and S. Levis (2012), A process-based fire parameterization of intermediate complexity in a Dynamic Global Vegetation Model, *Biogeosciences*, *9*, 2761–2780.
- Li, F., B. Bond-Lamberty, and S. Levis (2013), Quantifying the role of fire in the Earth system—Part 2: Impact on the net carbon balance of global terrestrial ecosystems for the 20th century, *Biogeosci. Discuss.*, *10*, 17,309–17,350.
- Liu, S., et al. (2011), Simulating the impacts of disturbances on forest carbon cycling in North America: Processes, data, models, and challenges, *J. Geophys. Res.*, *116*, G00K08, doi:10.1029/2010JG001585.
- Marlon, J. R., P. J. Bartlein, C. Carcaillet, D. G. Gavin, S. P. Harrison, P. E. Higuera, F. Joos, M. J. Power, and I. C. Prentice (2008), Climate and human influences on global biomass burning over the past two millennia, *Nat. Geosci.*, *1*, 697–702.
- Mitchard, E. T. A., S. S. Saatchi, A. Baccini, G. P. Asner, S. J. Goetz, N. L. Harris, and S. Brown (2013), Uncertainty in the spatial distribution of tropical forest biomass: A comparison of pan-tropical maps, *Carbon Balance Manage.*, *8*(10), 1–13.
- Mitchell, C. D., and P. Jones (2005), An improved method of constructing a database of monthly climate observations and associated high-resolution grids, *Int. J. Climatol.*, *25*, 693–712.
- Mouillot, F., and C. B. Field (2005), Fire history and the global carbon budget: A 1 × 1 fire history reconstruction for the 20th century, *Global Change Biol.*, *11*, 398–420.
- Mouillot, F., M. G. Schultz, C. Yue, P. Cadule, K. Tansey, P. Ciais, and E. Chuvieco (2014), Ten years of global burned area products from spaceborne remote sensing—A review: Analysis of user needs and recommendations for future developments, *Int. J. Appl. Earth Obs. Geoinf.*, *26*, 64–79.
- Murphy, B. P., J. Russell-Smith, and L. D. Prior (2010), Frequent fires reduce tree growth in northern Australian savannas: Implications for tree demography and carbon sequestration, *Global Change Biol.*, *16*, 331–343.
- Nowacki, G. J., and M. D. Abrams (2008), The demise of fire and “mesophication” of forests in the eastern United States, *BioScience*, *58*(2), 123–138.
- Page, S., F. Siegert, J. O. Rieley, H. D. V. Boehm, A. Jaya, and S. Limin (2002), The amount of carbon released from peat and forest fires in Indonesia during 1997, *Nature*, *420*, 61–65.
- Pan, Y., et al. (2011), A large and persistent carbon sink in the world's forests, *Science*, *333*, 988–993.
- Pechony, O., and D. T. Shindell (2009), Fire parameterization on a global scale, *J. Geophys. Res.*, *114*, D16115, doi:10.1029/2009JD011927.
- Peters, G. P., G. Marland, C. Le Quééré, T. A. Boden, J. G. Canadell, and M. R. Raupach (2011), Rapid growth in CO₂ emissions after the 2008–2009 global financial crisis, *Nat. Clim. Change*, *2*, 2–4.
- Pfeiffer, M., A. Spessa, and J. O. Kaplan (2013), A model for global biomass burning in preindustrial time: LPJ-LMfire (v1.0), *Geosci. Model Dev.*, *6*, 643–685.
- Piao, S. L., et al. (2013), Evaluation of terrestrial carbon cycle models for their response to climate variability and to CO₂ trends, *Global Change Biol.*, doi:10.1111/gcb.12187.
- Pison, I., P. Bousquet, F. Chevallier, S. Szopa, and D. A. Hauglustaine (2009), Multi-species inversion of CH₄, CO and H₂ emissions from surface measurements, *Atmos. Chem. Phys.*, *9*, 5281–5297.
- Plummer, S., et al. (2007), An update on the globcarbon initiative: Multi-sensor estimation of global biophysical products for global terrestrial carbon studies, in *ESA ENVISAT Symposium*, European Space Agency, Montreux, Switzerland.
- Poulter, B., S. Qian, and N. L. Christensen (2008), Determinants of coastal treelines, the role of abiotic and biotic interactions, *Plant Ecol.*, *202*(1), 55–66.
- Poulter, B., L. Aragão, J. Heinke, M. Gumpenberger, U. Heyder, A. Rammig, K. Thonicke, and W. Cramer (2010), Net biome production of the Amazon Basin in the 21st Century, *Global Change Biol.*, *16*(7), 2062–2075.
- Poulter, B., P. Ciais, E. L. Hodson, H. Lischke, F. Maignan, S. Plummer, and N. E. Zimmermann (2011), Plant functional type mapping for earth system models, *Geosci. Model Dev.*, *4*, 993–1010.
- Prentice, I. C., D. I. Kelley, P. N. Foster, P. Friedlingstein, S. P. Harrison, and P. J. Bartlein (2011), Modeling fire and the terrestrial carbon balance, *Global Biogeochem. Cycles*, *25*, GB3005, doi:10.1029/2010GB003906.
- Quegan, S., C. Beer, A. Shvidenko, I. McCallum, I. C. Handoh, P. Peylin, C. Rodenbeck, W. Lucht, S. Nilsson, and C. Schmullius (2011), Estimating the carbon balance of central Siberia using a landscape-ecosystem approach, atmospheric inversion and Dynamic Global Vegetation Models, *Global Change Biol.*, *17*, 351–365.
- Randerson, J. T., et al. (2006), The impact of boreal forest fire on climate warming, *Science*, *314*, 1130–1132.
- Randerson, J. T., Y. Chen, G. R. van der Werf, B. M. Rogers, and D. C. Morton (2012), Global burned area and biomass burning emissions from small fires, *J. Geophys. Res.*, *117*, G04012, doi:10.1029/2012JG002128.
- Rothermel, R. C. (1972), A mathematical model for predicting fire spread in wildland fuels, *Rep.*, Intermountain Forest and Range Experiment Station, Forest Service, U.S. Dept. of Agriculture, Ogden, Utah.
- Roy, D. P., and L. Boschetti (2009), Southern Africa validation of the MODIS, L3JRC, and GlobCarbon burned-area products, *IEEE Trans. Geosci. Remote Sens.*, *47*(4), 1032–1044.
- Roy, D. P., Y. Jin, P. E. Lewis, and C. O. Justice (2005), Prototyping a global algorithm for systematic fire-affected area mapping using MODIS time series data, *Remote Sens. Environ.*, *97*(2), 137–162.

- Ryan, K. C., E. E. Knapp, and J. M. Varner (2013), Prescribed fire in North American forests and woodlands: History, current practice, and challenges, *Front. Ecol. Environ.*, *11*, e15–e24.
- Saatchi, S. S., et al. (2011), Benchmark map of forest carbon stocks in tropical regions across three continents, *Proc. Natl. Acad. Sci. U.S.A.*, *108*(24), 9899–9904.
- Schultz, M. G., A. Heil, J. J. Hoelzemann, A. Spessa, K. Thonicke, J. Goldammer, A. C. Held, J. M. Pereira, and M. van het Bolscher (2008), Global emissions from wildland fires from 1960 to 2000, *Global Biogeochem. Cycles*, *22*, GB2002, doi:10.1029/2007GB003031.
- Schulze, E. D., C. Wirth, D. Mollicone, N. von Lupke, W. Ziegler, F. Achard, M. Mund, A. Prokushkin, and S. Scherbina (2012), Factors promoting larch dominance in Eastern Siberia: Fire versus growth performance and implications for carbon dynamics, *Biogeosciences*, *9*, 1405–1421.
- Sitch, S., et al. (2003), Evaluation of ecosystem dynamics, plant geography and terrestrial carbon cycling in the LPJ dynamic global vegetation model, *Global Change Biol.*, *9*, 161–185.
- Sitch, S., et al. (2013), Trends and drivers of regional sources and sinks of carbon dioxide over the past two decades, *Biogeosci. Discuss.*, *10*, 20,113–20,177.
- Staver, A. C., S. Archibald, and S. A. Levin (2011), The global extent and determinants of savanna and forest as alternative biome states, *Science*, *334*, 230–232.
- Takahashi, T., R. H. Wanninkhof, R. A. Feely, R. F. Weiss, D. W. Chipman, N. Bates, J. Olafsson, C. Sabine, and S. C. Sutherland (1999), Net sea-air CO₂ flux over the global oceans: An improved estimate based on the sea-air pCO₂ difference, paper presented at 2nd International Symposium, CO₂ in the Oceans, Center Global Env. Res., Tsukuba, Japan.
- Tansey, K., J. M. Gregoire, P. Defourny, E. G. Leigh, J. F. Pekel, E. van Bogaert, and E. Bartholome (2008), A new, global multi-annual (2000–2007) burnt area product at 1 km resolution, *Geophys. Res. Lett.*, *35*, L01401, doi:10.1029/2007GL031567.
- Taylor, K. E. (2001), Summarizing multiple aspects of model performance in a single diagram, *J. Geophys. Res.*, *106*(D7), 7183–7192, doi:10.1029/2000JD900719.
- Thonicke, K., S. Venevsky, S. Sitch, and W. Cramer (2001), The role of fire disturbance for global vegetation dynamics: Coupling fire into a Dynamic Global Vegetation Model, *Global Ecol. Biogeogr.*, *10*, 661–677.
- Thonicke, K., I. C. Prentice, and C. Hewitt (2005), Modeling glacial-interglacial changes in global fire regimes and trace gas emissions, *Global Biogeochem. Cycles*, *19*, GB3008, doi:10.1029/2004GB002278.
- Thonicke, K., A. Spessa, I. C. Prentice, S. P. Harrison, and C. Carmona-Moreno (2010), The influence of vegetation, fire spread and fire behaviour on biomass burning and trace gas emissions: Results from a process-based model, *Biogeosciences*, *7*, 1991–2011.
- van der Werf, G. R., J. T. Randerson, G. J. Collatz, and L. Giglio (2003), Carbon emissions from fires in tropical and subtropical ecosystems, *Global Change Biol.*, *9*, 547–562.
- van der Werf, G. R., J. T. Randerson, L. Giglio, G. J. Collatz, M. Mu, P. S. Kasibhatla, D. C. Morton, R. S. DeFries, Y. Jin, and T. T. van Leeuwen (2010), Global fire emissions and the contribution of deforestation, savanna, forest, agricultural, and peat fires (1997–2009), *Atmos. Chem. Phys.*, *10*, 11,707–11,735.
- Varner, J. M., F. E. Putz, J. J. O'Brien, R. J. Mitchell, J. K. Hiers, and D. R. Gordon (2009), Post-fire tree stress and growth following smoldering duff fires, *For. Ecol. Manage.*, *258*, 2467–2474.
- Venevsky, S., K. Thonicke, S. Sitch, and W. Cramer (2002), Simulating fire regimes in human-dominated ecosystems: Iberian Peninsula case study, *Global Change Biol.*, *8*, 984–998.
- Verdu, M., J. G. Pausas, J. G. Segarra-Moragues, and F. Ojeda (2007), Burning phylogenies: Fire, molecular evolutionary rates, and diversification, *Evolution*, *61*(9), 2195–2204.
- Yue, C., et al. (2014), Modelling fires in the terrestrial carbon balance by incorporating SPITFIRE into the global vegetation model ORCHIDEE—Part 1: Simulating historical global burned area and fire regime, *Geosci. Model Dev. Discuss.*, *7*, 1–51.
- Zhao, M., and S. W. Running (2010), Drought-induced reduction in global terrestrial net primary production from 2000 through 2009, *Science*, *329*(5994), 940–943.
- Zobler, L. (1986), A world soil file for global climate modeling, *NASA Tech. Memo.*, 32 pp.